Carbonates and Evaporites (2021) 36:71
https://doi.org/10.1007/s13146-021-00739-0

ORIGINAL ARTICLE

Hydro-geochemical evolution characteristics of shallow groundwater in northeast of Jianghan Plain, China

Meiyan Hu[1] · **Peijiang Zhou**[1]

Accepted: 1 August 2021 / Published online: 13 August 2021
© The Author(s), under exclusive licence to Springer-Verlag GmbH Germany, part of Springer Nature 2021

Abstract

Understanding the hydro-chemical evolution characteristics of groundwater is of great significance for the sustainable management and utilization of groundwater resources. In this study, the evolution characteristics of groundwater in northeast of Jianghan Plain were studied by hydro chemistry and isotope analysis, multivariate statistical analysis, and inverse geochemical modeling. First, a total of 130 groundwater samples were collected from three different aquifers for anion and cation analysis and hydrogen and oxygen isotopes analysis. Then the hydro-chemical type, composition, ion relationship, and evolution law of the three aquifers were discussed detailedly. Finally, inverse geochemical modeling and principal component analysis were carried out. The results show that the hydro-chemical types, anions and cations of the Holocene (Qh^{al}) aquifer in the study area are more diverse. The inverse geochemical model indicates that water–rock interaction is one of the factors affecting the chemical evolution of groundwater. The relatively higher concentrations of Na^+ and Cl^- in Paleogene (Ey) aquifer may be originated from the dissolution of saline minerals in red sandstone. The evaporation intensities of the three aquifers are controlled by the depth of the aquifer. Anthropogenic activities might have a greater effect on the Qh^{al} aquifer, but a less effect on the Ey aquifer. This work not only strengthens the understanding of groundwater evolution in this area, but also provides a reference for groundwater analysis in other similar areas.

✉ Peijiang Zhou
zhoupj@whu.edu.cn

Meiyan Hu
2018102050023@whu.edu.cn

[1] School of Resource and Environmental Science, Hubei Biomass-Resource Chemistry and Environmental Biotechnology Key Laboratory, Eco-Environment Technology R&D and Service Center, Wuhan University, Wuhan 430079, People's Republic of China

Graphic abstract

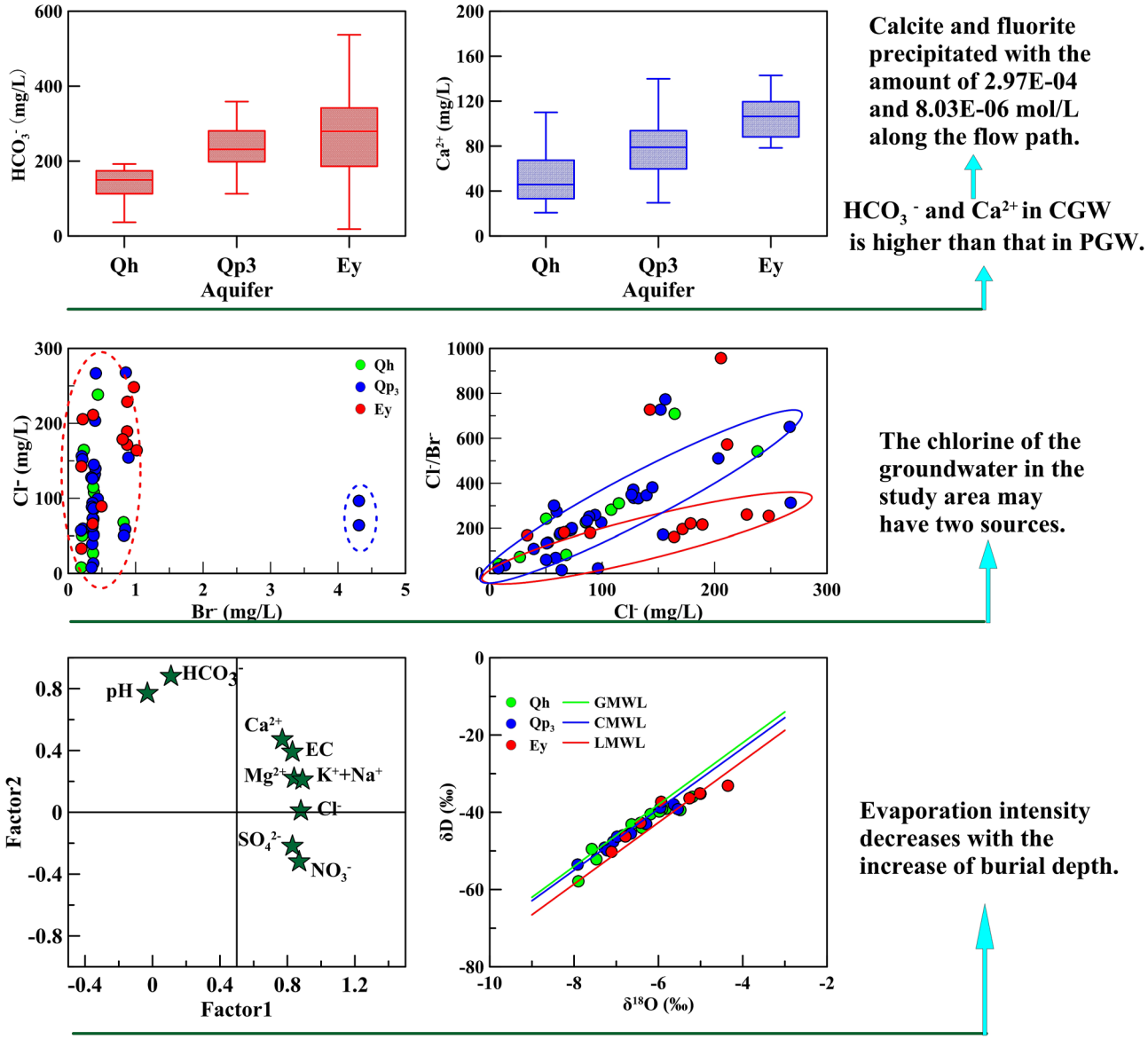

Keywords Hydro-geochemical evolution · Hydrochemistry · Principal component analysis (PCA) · Isotope · Inverse geochemical modeling

Introduction

Water resource plays a key role in consideration of human health, as well as ecological balance. To guarantee sustainable use of water, it is necessary to understand the groundwater recharge patterns and hydro-chemical characteristics. Many scholars have conducted profound studies in this field over recent years (Shi et al. 1998; Qin et al. 2005; Du et al. 2018a, b; Jiang et al. 2018).

Hydro chemical methods have been widely and successfully utilized to infer the source, recharge and mixing processes of groundwater, groundwater and surface water interactions along flow path, and anthropogenic activities impacts (Yangui et al. 2011). Therefore, chemical composition difference of different aquifers can be used to evaluate the hydro-geochemical evolution. The commonly used chemical methods are Piper diagram (Cates et al. 1996; Chadha 1999; Huang and Wang 2018; Mountadar et al. 2018) and ion ratio (Andersen et al. 2005; Ye et al. 2015; Adiya et al. 2017; Al-Mashakbeh 2017). Ion

ratios such as Cl/Br and Ca/Sr were utilized as tracers to investigate the origin of groundwater (Williams and Rodoni 1997; McGuire et al. 2002). Principal component analysis (PCA) has been applied to process real chemical data for the determination of temporal and spatial pattern of water chemistry (Christophersen and Hooper 1992; Momen et al. 1996). Using hierarchical cluster and principal component analysis (PCA), Yidana et al. (2008) and Rodriguez et al. (2016) selected the most representative wells of the region. Meanwhile, Kazakis et al. (2017) and Zhang et al. (2018) found high concentrations of NO_3^- in groundwater and heavy metals in soil, respectively.

Many researchers have evaluated and analyzed the hydrogeochemical evolution characteristics using isotopes (Barnes and Allison 1988; Aravena and Suzuki 1990; Williams and Rodoni 1997; Weyhenmeyer et al. 2002; Blasch and Bryson 2007; Lihe et al. 2010; Mokadem et al. 2016). Stable isotopes of oxygen and hydrogen in water have been used as space tracers to identify the origin of groundwater (Harford and Sparks 2001; van Geldern et al. 2014; Khalil et al. 2015; Ayadi et al. 2018). The inverse geochemistry modeling with PHREEQC has been tried to evaluate the hydro-geochemical evolution quantitatively (Lecomte et al. 2005; Yang et al. 2018). Some scholars have discovered the lithofacies change processes along the flow path using this method, such as silicate weathering and dissolution, and carbonate precipitation (Sharif et al. 2008; Gomaah et al. 2016; Slimani et al. 2017).

Jianghan Plain, located in the south central part of Hubei Province, is a low-lying alluvial plain formed by the Yangtze River and Hanjiang River, covering an area of 55,000 km^2. Gan et al. (2014) and Niu et al. (2017) summarized the regional chemical characteristics by means of hydro-chemical constant analysis. Using isotope tritium simulation, Du et al. (2018a, b) concluded the interaction between different shallow aquifers in Jianghan Plain. Zhou et al. (2013) and Yang et al. (2020) analyzed the geochemical and anthropogenic processes by multivariate statistical method, and identified the temporal and spatial patterns and the controlling factors of groundwater geochemistry.

In this paper, hydrochemistry, isotope, principal component analysis (PCA), and inverse geochemistry modeling were used to comprehensively analyze the hydro-geochemical evolution characteristics of shallow groundwater in the northeast of Jianghan Plain. This study is helpful to understand the hydrogeochemical evolution characteristics of groundwater in Jianghan Plain, and provides a significant guidance and reference for carrying out regional groundwater research with comprehensive methods.

Hydrogeological setting

The study area is located in the northeast of Jianghan Plain (Fig. 1b). It is a terrain turning zone in the mountain and the plain, covering approximately 460 km^2, with a low hilly plain in north and a valley plain in south. Huan-river is the main river which crosses over the middle of the study area from north to south. The study area belongs to subtropical continental monsoon climate with two distinct seasons, a rainy season from April to August and a dry season from September to March. The monthly average temperature is higher during the rainy season (> 15 °C) and lower during the dry season (< 15 °C). The minimum temperature is around 5 °C recorded in January and the maximum temperature is around 28 °C recorded in July (Fig. 2). The annual average rainfall is 1200 mm, and the evaporation is 1435 mm, which is slightly larger than the rainfall (Fig. 2). These climatic conditions maintain the agriculture type of dry field combined with paddy field, with cotton, peanut, maize and rice as the main crops.

The study area is mainly underlain by the Sandstone of Paleogene (Ey), and about 95% of the surface is covered by weathering of Quaternary (Upper Pleistocene Qp_3^{al} or Holocene Qh^{al}). The stratigraphic structure on the east and west sides of the Huan River in the study area is roughly symmetrical. The weathering zone on the east side of the Huan River is composed of a double-layer structure gradually thickened from northeast to southwest, with a thickness of 1–30 m (Fig. 3). The upper layer is composed of sand and clay containing gypsum with a thickness of about 5–20 m. Therefore, this layer may be a representative of aquitard and lead to the existence of confined conditions in most parts of aquifer system. The layer below is sand-gravel with thickness between 5 and 10 m. Previous studies have indicated that Jianghan Plain is a typical carbonate (dolomite or calcite) weathering zone (Zhou et al. 2013). Sericite, quartz, and a small amount of halite and fluorite were also found in the study area during the field investigation. The weathering and lixiviation process of fluorine minerals in rocks and soils led to the release of considerable quantity of fluorine into groundwater, which resulted in the relatively high concentration of fluorine in clay and groundwater in Jianghan Plain (Zeng 1997).

The upper layer in the study area is composed of Upper Pleistocene sediments (clay and gravelly sand), or Holocene sediments (silty clay and gravel), functioning as porous media for groundwater storage and flow, and the primary layer for local water supply, with thickness ranging from 1 to 40 m. The underlying layer is composed of

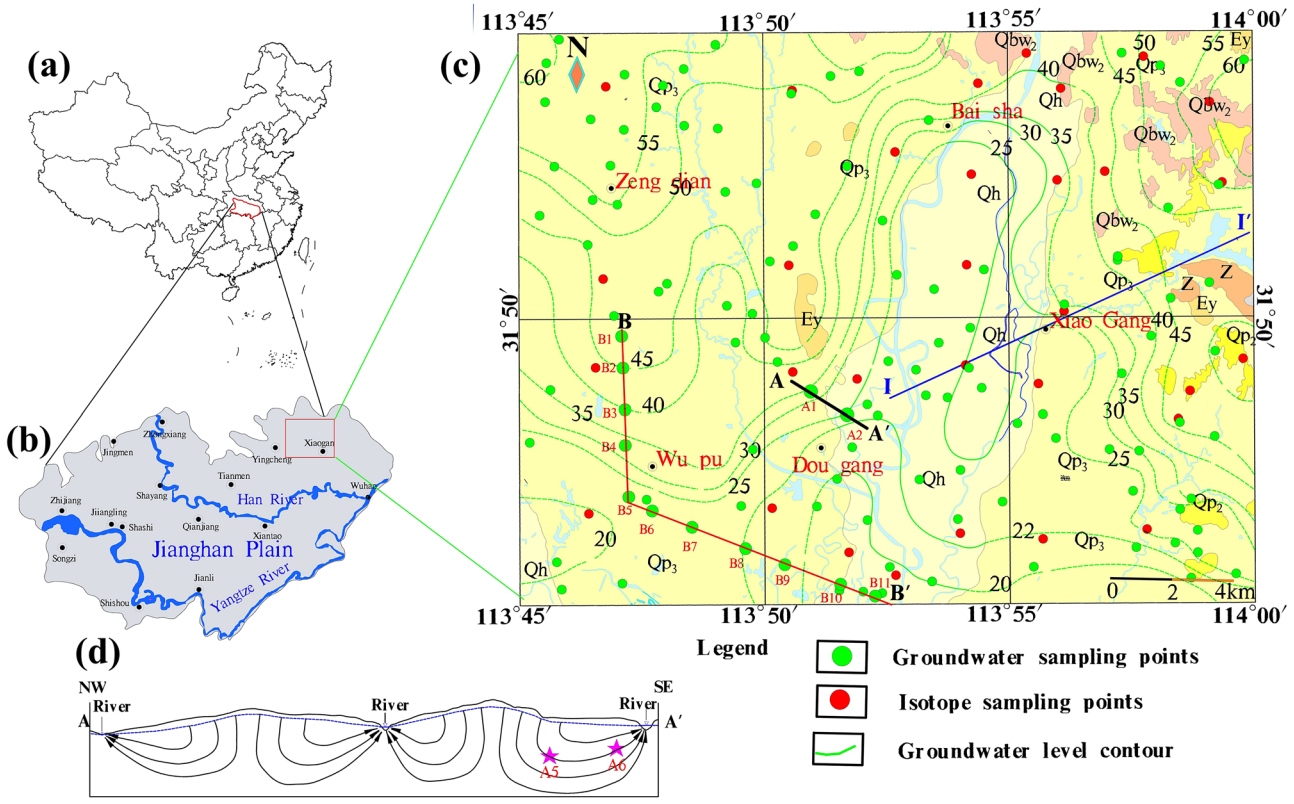

Fig. 1 **a** The geographic location of the Jianghan Plain; **b** the geographic location of the study area; **c** location of study area and distribution of sampling points; **d** groundwater flow pattern of section A–A′ in study area

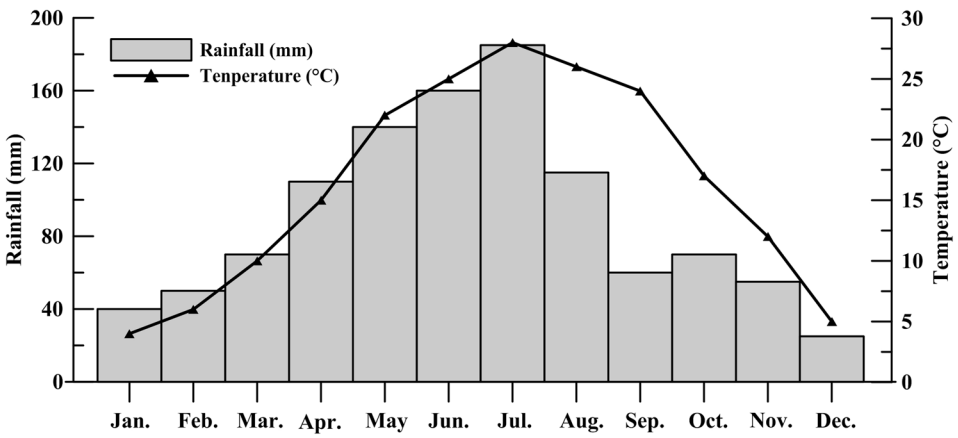

Fig. 2 The average monthly rainfall and temperature in the study area (Dawu station from 1981 to 2010)

Paleogene (red sandstone) with a thickness of 50–80 m, which is conducted as the second aquifer. Groundwater is mainly recharged by atmospheric precipitation or surface water, and is drained by rivers or wells mostly.

Methodology

Data preparation

Data used in this study were self-tested. The information of all data collected is summarized in Table 1. Ninety-eight groundwater samples were sampled (Fig. 1c) for chemical composition analysis from the study area from

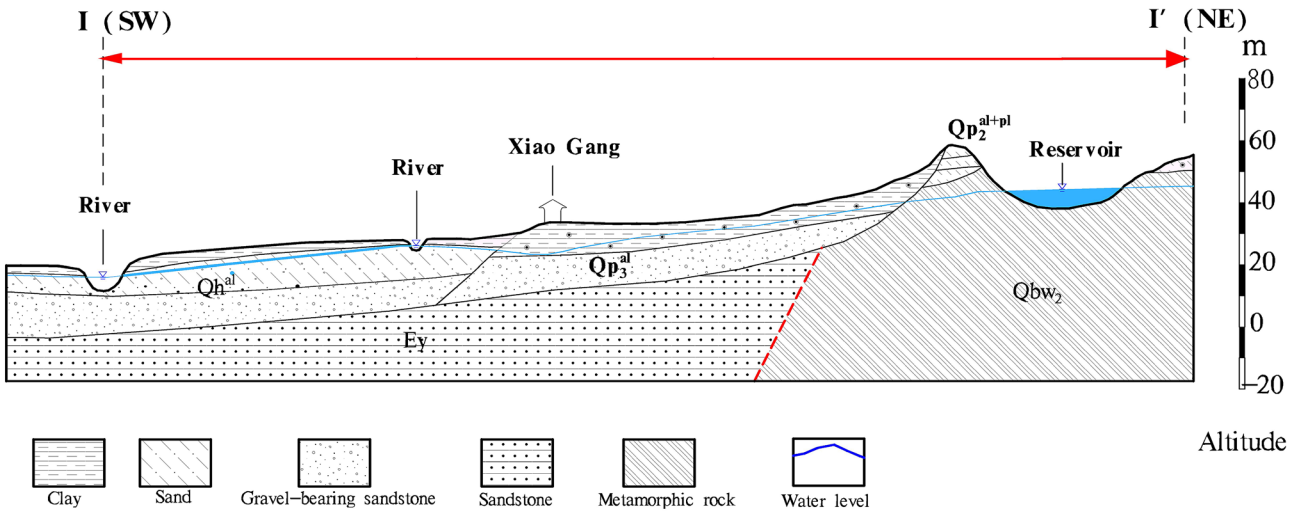

Fig. 3 Hydrogeological profile I–I′ in the study area

Table 1 Information of data collected in this study

Parameters	Aquifer	*N*	Time	Data source
Chemical composition (98)				
pH, EC, TDS, HCO_3^-, Cl^-, Br^-, F^-, NO_3^-, SO_4^{2-}, Ca^{2+}, Mg^{2+} Na^+ and K^+	Qh^{al}	24	2016.9–2016.10	Self-test
	$Qp_3{}^{al}$	56	2016.9–2016.10	Self-test
	Ey	18	2016.9–2016.10	Self-test
Isotopic composition (32)				
^{18}O and ^2H	Qh^{al}	12	2016.9–2016.10	Self-test
^{18}O and ^2H	$Qp_3{}^{al}$	13	2016.9–2016.10	Self-test
^{18}O and ^2H	Ey	7	2016.9–2016.10	Self-test

September to October 2016. Among them, 24 samples were taken from Qh^{al} aquifer, 56 samples were taken from $Qp_3{}^{al}$ aquifer, and the left 18 were taken from Ey aquifer. Groundwater samples were taken from hand-pumped wells or motor-pumped wells. Before sampling, the wells and boreholes were purged by pumping until the temperature, pH, and electrical conductivity (EC) were stable. Total dissolved solids, pH and EC were measured on site using a portable TDS, pH and EC meter. Concentrations of HCO_3^- were measured within 24 h using acid–base titration methods. Cations of Ca^{2+}, Mg^{2+} Na^+, and K^+ were determined in the laboratory using an inductively coupled plasma atomic emission spectrometer (ICP-AES) (IRIS Intrepid II XSP, USA). Anions such as Cl^-, Br^-, NO_3^-, and SO_4^{2-} were determined using an ion chromatograph (Dionex 2500, USA). The analytical precision reported by the laboratories was better than 5%.

In addition, thirty-two groundwater samples were sampled (Fig. 1) for isotopes composition analysis from the study area from September to October 2016. Among them, 12 samples were taken from Qh^{al} aquifer, 13 samples taken from $Qp_3{}^{al}$ aquifer, and the left 7 were taken from Ey aquifer. Hydrogen/Oxygen (H/O) isotopes were measured using a gas stable isotope mass spectrometer (MAT253, Finnigan, Germany). The precisions for $\delta^{18}O$ and δ^2H were $\pm 0.1‰$ and $\pm 1.0‰$, respectively.

Data analysis

Different kinds of methods were used to evaluate the hydrogeochemical evolution characteristics of groundwater in the area, including conventional hydrochemistry (Piper diagram, box diagram, ion ratio), and multivariate statistical analysis–principal component analysis. Furthermore, inverse geochemistry modeling was performed along the selected path using PHREEQC to assess the evolution characteristics quantitatively.

Chemical composition and isotopic composition analysis

The differences of hydro-chemical composition and D–O isotopic composition in different aquifers were compared and analyzed by mapping method (mainly including Piper diagram, box plot, line plot, scatter plot, etc.). In addition, proportional

coefficient method (such as Cl/Br) was used to discuss the source of hydro-chemical composition in different aquifers.

Inverse geochemistry modeling

Inverse geochemical modeling is usually used to establish hydro-geochemical evolution models to quantitatively calculate mineral mass transfer from one site to another on the same flow path (Sharif et al. 2008; Bretzler et al. 2011). Its basic principle that is the mass of hydro-chemical composition at the end point is equal to that of the starting point plus the transfer amount between two points due to water–rock interaction along the same groundwater flow path. Based on the mass balance and charge balance reaction model, it can be inferred that the hydro-geochemical reaction from the beginning to the end of groundwater can be expressed as following:

$$\begin{cases} \sum_{p=1}^{p} a_p b_p, k = mT, K(\text{Ending}) - mT, K(\text{Starting}) \\ \sum_{p=1}^{p} u_p a_p = \Delta \text{RS} \end{cases}, \quad (1)$$

where p is referred to the number of mineral phases; a_p is the number of moles of the mineral phase p entering or leaving the solution per liter; b_{pk} is the stoichiometric number of the element k in the mineral phase p; MT, K is the molar concentration of the element k; up is the effective valence state of the mineral phase p; δRS is redox state.

To quantitatively analyze the water–rock interaction between Qp_3^{al} and Qh^{al} aquifers in the study area, PHREEQC was applied to inverse geochemical modeling. Therefore, the path A1 → A2 from Qp_3^{al} to Qh^{al} was selected along the groundwater flow direction based on the groundwater level contour measured in September 2016 (Fig. 1d).

Based on the hydro geochemistry, lithology and mineral constituent, the possible minerals such as calcite, dolomite, fluorite, gypsum, and halite were selected. In addition, cation exchange reactions might occur in the groundwater system according to the distribution characteristics of cations (Table 2). Moreover, it was negligible of the existence of CO_2 since the simulated flow path in the study area can be considered as a closed system.

Seven elements of Na, Ca, Mg, C, S, F, and Cl were considered as constraints variables according to the test results of hydrochemistry in the study area (Table 3). Model was established based on the selected mineral phases and main target elements (Eqs. 2–8).

$$\text{Halite} + \text{NaX} = \Delta M(\text{Na}), \quad (2)$$

$$\text{Caclite} + \text{Dolomite} + \text{Gypsum} + \text{Fluorite} + \text{CaX}_2 = \Delta M(\text{Ca}), \quad (3)$$

Table 2 The equation of mineral reaction

Mineral phase	Chemical formula	Chemical reaction
Calcite	$CaCO_3$	$CaCO_3 == Ca^{2+} + CO_3^{2-}$
Dolomite	$CaMg(CO_3)_2$	$CaMg(CO_3)_2 == Ca^{2+} + Mg^{2+} + 2CO_3^{2-}$
Gypsum	$CaSO_4 \cdot 2H_2O$	$CaSO_4 \cdot 2H_2O == Ca^{2+} + SO_4^{2-} + 2H_2O$ $CaSO_4 == Ca^{2+} + SO_4^{2-}$
Fluorite	CaF_2	$CaF_2 == Ca^{2+} + 2F^-$
Halite	NaCl	$NaCl == Na^+ + Cl^-$
Exchange ion	NaX, CaX_2	$Ca^{2+} + 2Na == Ca + 2Na^+$

$$\text{Dolomite} = \Delta M(\text{Mg}), \quad (4)$$

$$\text{Caclite} + \text{Dolomite} = \Delta M(\text{C}), \quad (5)$$

$$\text{Gypsum} = \Delta M(\text{S}), \quad (6)$$

$$\text{Flurite} = \Delta M(\text{F}), \quad (7)$$

$$\text{Halite} = \Delta M(\text{Cl}). \quad (8)$$

Principal component analysis

Principal component analysis (PCA) is a statistical method for dimensionality reduction. With the help of an orthogonal transformation, it transforms the original random vectors whose components are correlated into new random vectors whose components are not correlated. Usually, the mathematical treatment is to make a linear combination of the original indexes as a new comprehensive index.

$$Fp = a1i\text{ZX}1 + a2i\text{ZX}2 + \ldots\ldots + api\text{ZX}p, \quad (9)$$

where p refers to the p-th principal component extracted; $a1i$, $a2i$…, api ($I = 1\ldots, m$) is the covariance matrix of the corresponding eigenvectors; ZX_1, ZX_2…, ZX_p, are the normalized values of the original variables.

Taking pH, EC, HCO_3^-, Cl^-, NO_3^-, SO_4^{2-}, Ca^{2+}, Mg^{2+}, and $Na^+ + K^+$ into account for principal component analysis (PCA) with SPSS20 based on 98 groundwater samples in the whole area. Then, the principal component analysis was carried out based on 24 samples in Qh^{al} aquifer, 56 samples in Qp_3^{al} aquifer and 18 samples in Ey aquifer, respectively.

Table 3 Chemical composition of start and end points on the simulated path

Sample No.	Aquifer	pH	HCO_3^- (mg/L)	Ca^{2+} (mg/L)	Cl^- (mg/L)	F^- (mg/L)	Mg^{2+} (mg/L)	Na^+ (mg/L)	SO_4^{2-} (mg/L)
A1	Qp_3^{al}	6.95	335.610	63.74	49.03	0.307	17.71	55.11	30.15
A2	Qh^{al}	7.25	265.362	55.42	45.69	0.002	13.19	50.63	27.63

Results

Chemical composition of groundwater

The descriptive statistics of the chemical composition of groundwater in different aquifers are shown in Table 4. Groundwater samples from three aquifers are slightly acidic to slightly alkaline with pH values in the ranges of 6.04–7.31, 6.48–7.82, and 6.64–8.05, respectively. The EC values vary from 183 to 1430 μs/cm for Holocene (Qh^{al}), from 169 to 1544 μs/cm for Upper Pleistocene (Qp_3^{al}), and from 271 to 1335 μs/cm for Paleogene (Ey). The TDS values of the Qh^{al}, Qp_3^{al}, and Ey are 153–1091, 162–1391, and 233–1002 mg/L, respectively.

The hydro-chemical types in Upper Pleistocene (Qp_3^{al}) and Paleogene (Ey) aquifers are mainly HCO_3–Ca–Na type and HCO_3–Cl–Ca–Na type. While, there are three water types of HCO_3–Cl–Ca–Mg, HCO_3–Ca–Mg, and HCO_3–Cl–Ca–Na–Mg in Holocene (Qh^{al}) aquifer (Table 4 and Fig. 4). The main anions are HCO_3^- and Cl^-, and the main cations are Ca^{2+} and Na^+ in Qp_3^{al} and Ey aquifers. However, in Qh^{al} aquifer, anions, cations, and hydro-chemical types are more diverse.

The concentrations of HCO_3^- and Ca^{2+} in Upper Pleistocene (Qp_3^{al}) and Paleogene (Ey) aquifers are greater than that of Holocene (Qh^{al}) aquifer (Fig. 5). Table 5 and Fig. 6a show that the ranges of Cl^- concentration in Qh^{al} aquifer and Qp_3^{al} aquifer are 8.06–238.21 mg/L and 39.19–203.39 mg/L, respectively. Figure 6b shows that the concentration of Br^- in the three aquifers is close to 0.5 mg/L, except for two samples collected from unsealed wells in Qp_3^{al} aquifer. The concentration of Br^- in two unsealed wells reaches to 4.5 mg/L, which may be related to human pollution. The relationships of different major ions are shown in Fig. 7. Most groundwater samples in the three aquifers are close to the equal concentration (1:1) line, while the concentrations of Na^+ and Cl^- in Ey aquifer seem to be higher than that in the other two aquifers (Fig. 7a). In addition, a relatively large number of groundwater samples in the three aquifers are below the equal concentration (1:1) line of the Cl^- and HCO_3^-, and, moreover, almost all samples are above the equal concentration line of the Cl^- and SO_4^{2-}, indicating that HCO_3^- is the most abundant anion in the study area (Fig. 7c, d).

Isotopic composition of groundwater

Water stable isotopes ($\delta^{18}O$ and δ^2H) play a key role in tracing the hydrological processes (Clark and Fritz 1997). The values of $\delta^{18}O$ and δ^2H of different aquifers in the study area are listed in Table 6. The means of $\delta^{18}O$ are −6.44, −6.51, and −5.84‰, and the average values of δ^2H in the three aquifers are −43.86, −44.24, and −40.16‰, respectively. The similarity between $\delta^{18}O$ and δ^2H values in the three aquifers illustrates that there is a hydraulic connection among the three aquifers (Fig. 8).

Gan et al. (2014) summarized and analyzed the China meteoric water line (CMWL, $\delta^2H = 7.9\ \delta^{18}O + 8.2$) and the local meteoric water line (LMWL, $\delta^2H = 7.96\ \delta^{18}O + 5.1$). Compared with CMWL, the slope of LMWL located below is slightly higher, which indicates that not only the evaporation intensity of precipitation is higher, but also the heavy oxygen isotopes are more enriched in the region.

Based on the least squares regression, the parameters of the best-fit regression line for different aquifers were calculated (Table 6). The fitting equations of evaporation line are expressed as $\delta^2H = 7.24\ \delta^{18}O + 2.75$ ($R^2 = 0.922$), $\delta^2H = 6.41\ \delta^{18}O - 2.47$ ($R^2 = 0.976$), and $\delta^2H = 6.04\ \delta^{18}O - 5.35$ ($R^2 = 0.923$) in Qh^{al}, Qp_3^{al}, and Ey aquifers, respectively.

Table 4 Basic chemical composition in different aquifers in the study area

Aquifer type	pH	EC (μs/cm)	TDS (mg/L)	Chemical type
Holocene (Qh^{al})	6.04–7.31	183–1430	153–1091	HCO_3–Cl–Ca–Mg HCO_3–Ca–Mg HCO_3–Cl–Ca–Na–Mg
Upper pleistocene (Qp_3^{al})	6.48–7.82	169–1544	162–1391	HCO_3–Ca–Na HCO_3–Cl–Ca–Na
Paleogene (Ey)	6.64–8.05	271–1335	233–1002	HCO_3–Ca–Na HCO_3–Cl–Ca–Na

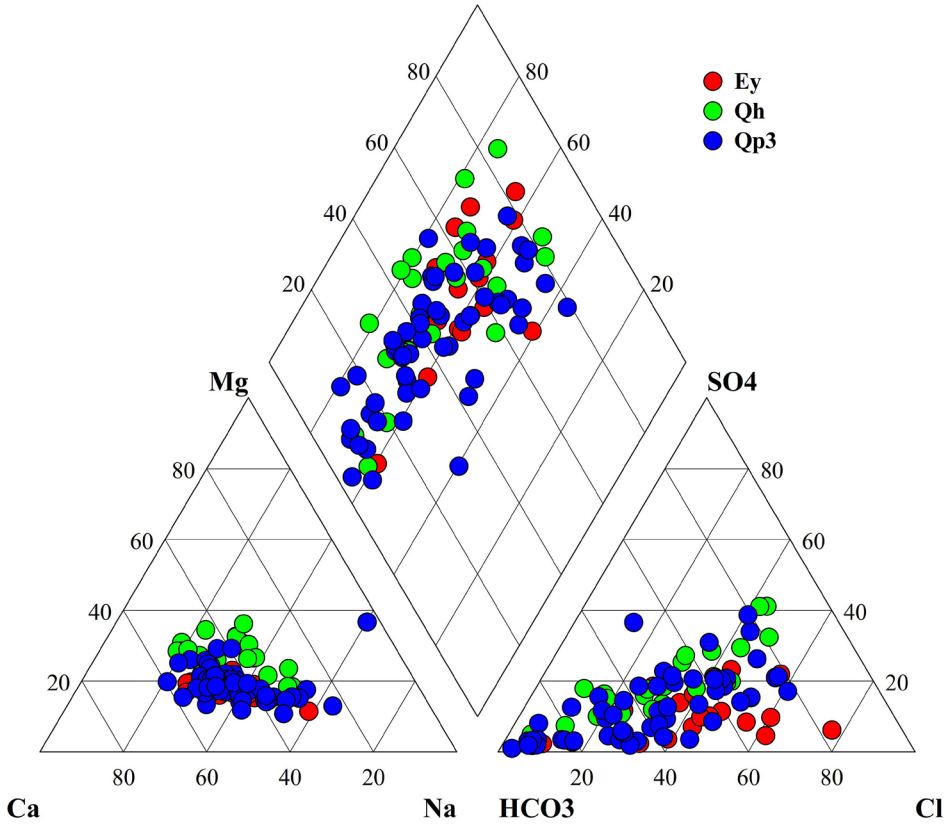

Fig. 4 Projection of water samples in the Piper diagram

Results of inverse geochemistry modeling

Table 7 shows the calculated saturation index of the start and end points on the simulated path. It is difficult to select the optimal solution due to the multiple solutions in inverse geochemical modeling. (Lecomte et al. 2005). Therefore, these factors, including thermodynamic balance, element adsorption affinity, hydro-chemical evolution characteristics, and mineral saturation index, should be comprehensively considered when the optimal solution is selected.

Along the path A1 (Qp_3^{al}) → A2 (Qh^{al}), eight solutions of the model were calculated (Table 8). Based on the variation of hydro-chemical characteristics from the Qp_3^{al} aquifer to the Qh^{al} aquifer, it is speculated that the cation exchange reaction may occur, but the reaction is not involved in solutions 2, 3, 6, and 7 (Table 8). According to Tables 7 and 3, the saturation index of calcite increases significantly from negative value to positive value, and the concentration of HCO_3^- and Ca^{2+} decreases along the path, indicating that calcite phase has a precipitation tendency. But calcite precipitation does not occur in solutions 2, 5, 7, and 8, as shown in Table 8. In addition, it seems impossible for halite to precipitate in natural environment due to the high solubility, but there is the appearance of the halite precipitation in solutions 1, 3, 5, and 7. The concentration of F^- decreases significantly, which suggests that fluorite precipitation may occur. Table 8 shows that all solutions in the model involve fluorite precipitation reaction, which is consistent with the inference. Based on the above analysis, solution 4 may be the most suitable solution of the model (Eqs. 10–12). The reaction processes on the simulated flow path can be summarized as following: calcite and fluorite are precipitated with the amount of 2.97E−04 and 8.03E−06 mol/L, respectively. Meanwhile, Ca–Na cation exchange reaction occurs with 9.74E−05 mol/L Ca^{2+} released into groundwater and 1.95E−04 mol/L Na^+ precipitated out from groundwater.

$$Ca^{2+} + CO_3^{2-} = CaCO_3, \tag{10}$$

$$Ca^{2+} + 2F^- = CaF_2, \tag{11}$$

$$Ca^{2+} + 2Na = Ca + 2Na^+. \tag{12}$$

Results of principal component analysis

The correlation matrix of chemical components for all groundwater samples in the study area was got by principal component extraction and maximum variance orthogonal rotation, as shown in Table 9. The Kaiser–Meyer–Olkin (KMO) test value is 0.775, and the Bartlett test level is 0.00,

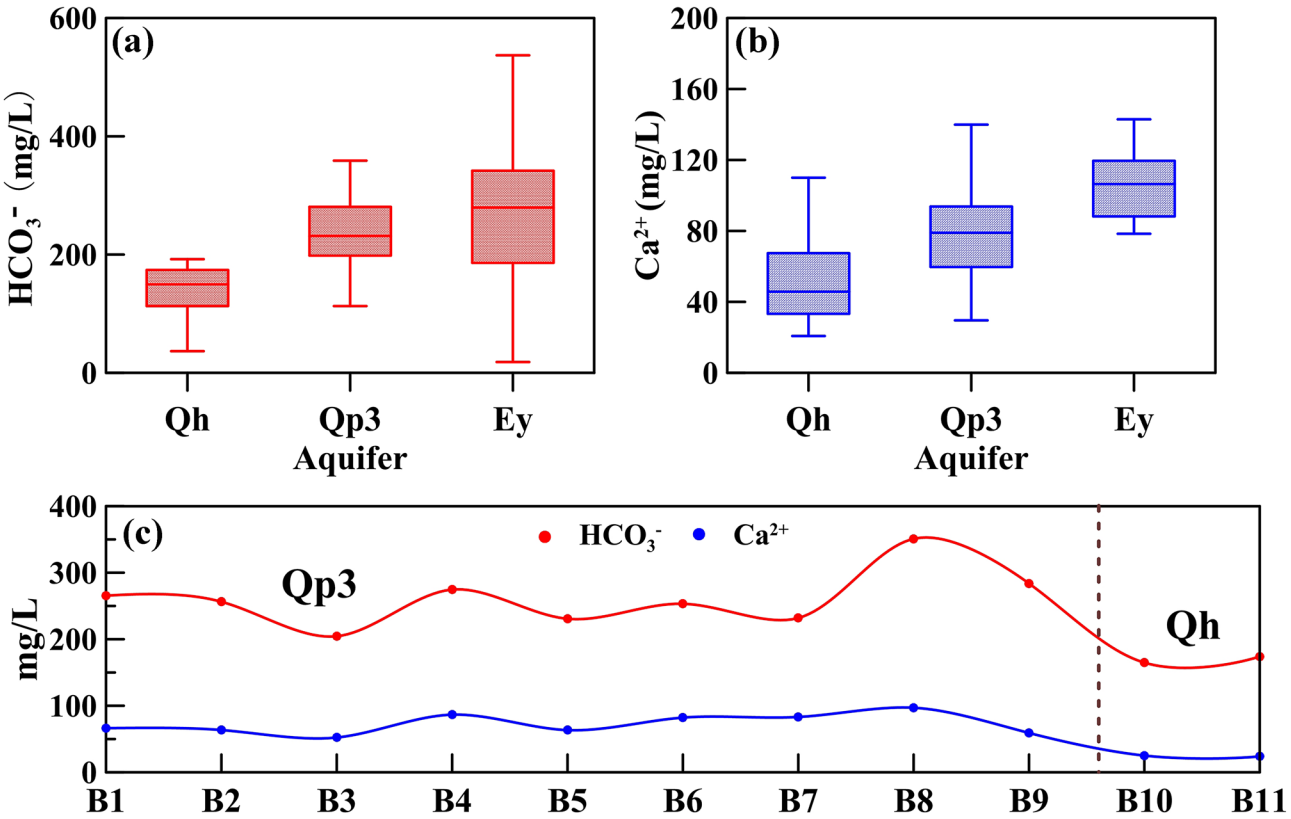

Fig. 5 The concentrations of HCO_3^- and Ca^{2+}: **a** box plot of HCO_3^-, **b** box plot of Ca^{2+}, and **c** concentration variations of HCO_3^- and Ca^{2+} in profile B–B′

Table 5 Analysis of Cl^- concentration of different aquifers in the study area

Aquifer	Cl^- concentration		
	Maximum (mg/L)	Minimum (mg/L)	Average (mg/L)
Qh^{al}	238.21	8.06	92.02
Qp_3^{al}	203.39	39.19	94.73
Ey	248.15	33.34	160.70

which indicates that the calculation results are suitable for principal component analysis. Table 9 reflects that there are obvious correlations among EC, Ca^{2+}, Mg^{2+}, $Na^+ + K^+$, Cl^-, NO_3^- and SO_4^{2-}.

Rotation factor load matrix of chemical components in groundwater was got by further dimension reduction analysis (Table 10). When the eigenvalue was set to 1, two factors were selected, and the cumulative contribution rate reaches to 77.782%, which reflects 77.782% of the sample information.

Factor 1 is composed of EC, Cl^-, NO_3^-, SO_4^{2-}, Ca^{2+}, Mg^{2+} and $Na^+ + K^+$ (Fig. 9), whose factor loads are all above 0.75, and the cumulative contribution rate reaches to 57.338%. Among them, Ca^{2+}, Mg^{2+}, Na^+ and K^+ may originate from the dissolution of some sedimentary rocks. SO_4^{2-} may come from sulfate deposits in various sedimentary rocks or sulfur compounds in pesticides, which is consistent with Du et al. (2017). Cl^- and NO_3^-, conservative components in groundwater, which do not participate in chemical weathering, may come from anthropogenic activities impacts, such as fertilizers, pesticides or excreta of human beings. The above analysis shows that the hydrochemistry in the study area is mainly affected by the geological background and anthropogenic activities.

Factor 2 includes pH and HCO_3^- with factor loads greater than 0.75, and the cumulative contribution rate is 20.444%. The compositions of factor 2 indicate that the degree of acid and alkaline and the balance of carbonate have a certain degree of effect on the evolution of groundwater chemical composition.

In addition, principal component factor analysis was carried out for the water samples from three aquifers in the study area (Table 11). In the Qh^{al} and Qp_3^{al} aquifers, two factors were selected with cumulative contribution rates of 87.964% and 75.425%, respectively. However, three factors were selected in Ey aquifer, and the cumulative contribution rate is 84.635%, reflecting 84.635% of the sample information.

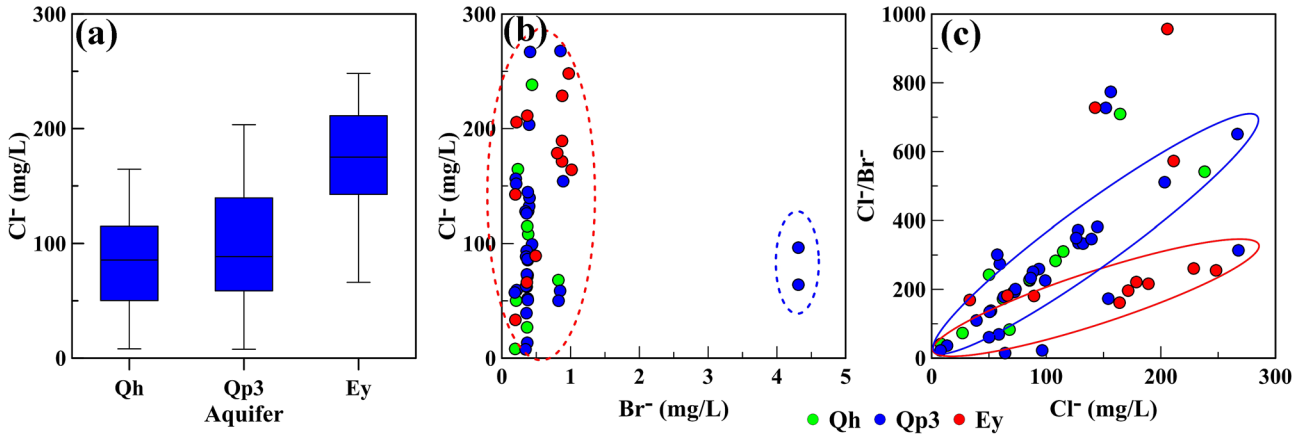

Fig. 6 The relationship between Cl^- and Br^-: **a** box plot of Cl^-, **b** mass ratio of Cl^- and Br^-, and **c** relationship between Cl^-/Br^- and Cl^-

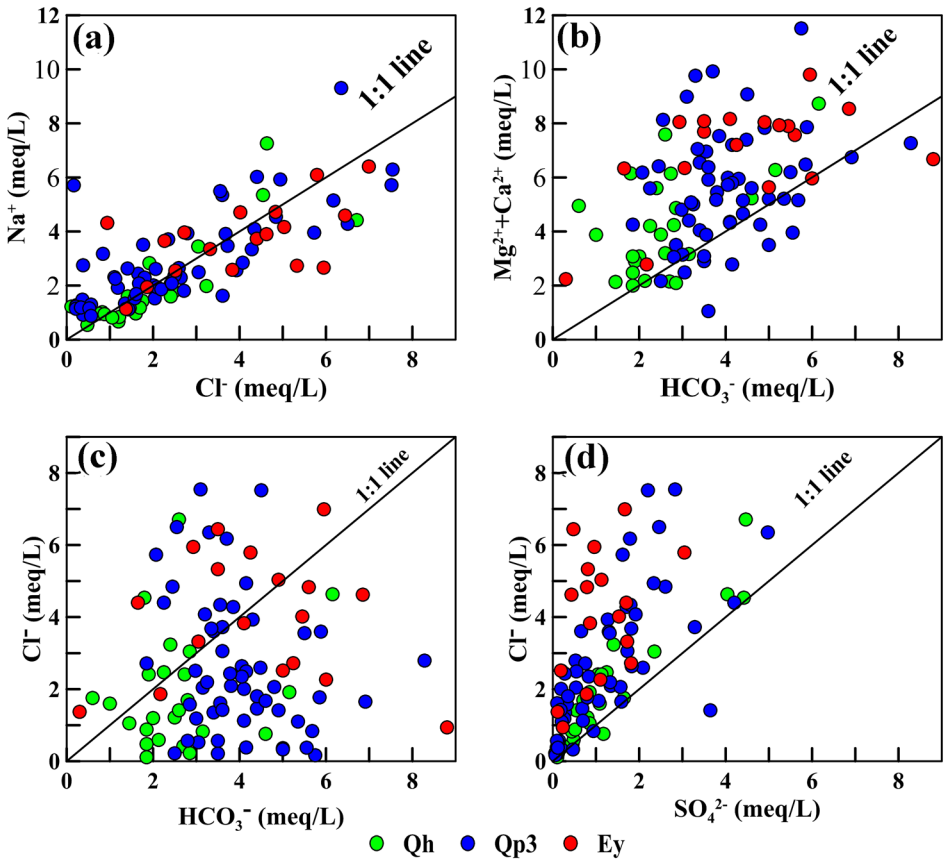

Fig. 7 The relationships of different major ions: **a** Na^+/Cl^-, **b** $Mg^{2+}+Ca^{2+}/HCO_3^-$, **c** Cl^-/HCO_3^-, and **d** Cl^-/SO_4^{2-}

Table 6 Isotopic composition and analysis

Aquifer	Burial depth (m)	$\delta^{18}O$ (‰)		$\delta^{2}H$ (‰)		Slope of evaporation line (K)	Intersection (d)	Coefficient of determination (R^2)
		Range (min, max)	Average	Range (min, max)	Average			
Qh^{al}	1–10	−7.90, −5.19	−6.44	−57.84, −35.96	−43.86	7.24	2.75	0.922
Qp_3^{al}	8–18	−7.91, −5.00	−6.51	−53.55, −35.19	−44.24	6.41	−2.47	0.976
Ey	15–35	−7.11, −4.35	−5.84	−50.24, −33.14	−40.16	6.04	−5.35	0.923

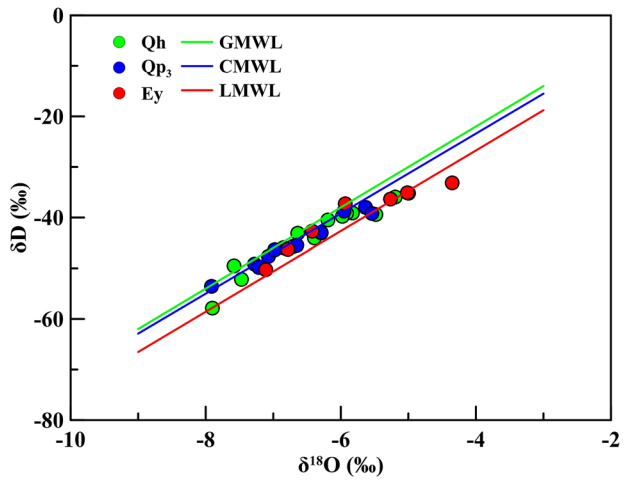

Fig. 8 Comparison on δ^2H–$\delta^{18}O$ of the groundwater samples in study area with the global meteoric water line (GMWL), China meteoric water line (CMWL) and local meteoric water line (LMWL)

Table 7 Saturation index of start and end points on the simulated path

Sample No.	Calcite	Dolomite	Fluorite	Gypsum	Halite
A1	−0.13	−0.47	−2.11	−2.18	−7.14
A2	0.03	−0.22	−6.51	−2.24	−7.20

Discussion

The higher concentrations of bicarbonate and calcium in shallow groundwater are typical characteristics of groundwater affected by water–carbonate mineral interactions (Du et al. 2017). Figures 4 and 5 show that the concentrations of $Mg^{2+}+Ca^{2+}$ and HCO_3^- in Qh^{al} aquifer are generally lower than that in the other two aquifers. Meanwhile, anions, cations and hydro-chemical types in Qh^{al} aquifer are more diverse. There are two possibilities for this phenomenon: one is that the Qh^{al} aquifer is more likely to be affected by agricultural activities owing to the thin sediments and strong permeability, and the other is that the Qh^{al} aquifer is recharged by other waters, resulting in the increase of Mg^{2+} and hydro-chemical types (Du et al. 2018a, b). It is inferred that CO_3^{2-} derived from HCO_3^- may combine with Ca^{2+} and precipitate during runoff process, resulting in the decrease of concentrations of Ca^{2+} and HCO_3^- in groundwater (Zhou et al. 2013). The CO_3^{2-} converted from HCO_3^- may be combined with Ca^{2+} and precipitated when the groundwater in Qh^{al} aquifer was recharged by the lateral runoff of other aquifers, resulting in relatively small concentration of Ca^{2+} and HCO_3^- in the aquifer (Fig. 5c). This can be confirmed by the reverse geochemistry modeling results. When groundwater flows between Qp_3^{al} aquifer and Qh^{al}

Table 8 Simulation result on path A5 → A6 using PHREEQC

Phase	Solution 1	Solution 2	Solution 3	Solution 4	Solution 5	Solution 6	Solution 7	Solution 8
Calcite	−2.50E−04	–	−2.00E−04	−2.97E−04	–	−2.00 E−04	–	–
Dolomite	–	–	–	–	–	–	–	–
Fluorite	−8.03E−06	−8.03E−06	−8.03E−06	−8.03E−06	−8.03E−06	−8.03E−06	−8.03E−06	−8.03E−06
Gypsum	–	–	–	–	–	–	–	–
Halite	−9.42E−05	–	−9.42E−05	–	−9.42E−05	–	−8.03E−06	–
CaX_2	5.03E−05	–	–	9.74E−05	5.03E−05	–	–	9.74E−05
NaX	−1.01E−04	–	–	−1.95E−04	−1.01E−04	–	–	−1.95E−04

Table 9 Correlation matrix of groundwater parameters

	pH	EC (μs/cm)	HCO_3^- (mg/L)	Cl^- (mg/L)	NO_3^- (mg/L)	SO_4^{2-} (mg/L)	Ca^{2+} (mg/L)	Mg^{2+} (mg/L)	K^++Na^+ (mg/L)
pH	1.00								
EC (μs/cm)	0.23	1.00							
HCO_3^- (mg/L)	0.47	0.37	1.00						
Cl^- (mg/L)	0.05	0.72	0.04	1.00					
NO_3^- (mg/L)	−0.21	0.55	−0.17	0.74	1.00				
SO_4^{2-} (mg/L)	−0.09	0.54	−0.06	0.63	0.75*	1.00			
Ca^{2+} (mg/L)	0.20	0.82*	0.51	0.71*	0.51	0.41	1.00		
Mg^{2+} (mg/L)	0.06	0.75*	0.33	0.64	0.63	0.68	0.76*	1.00	
K^++Na^+ (mg/L)	0.19	0.81*	0.29	0.77*	0.71*	0.74*	0.69	0.69	1.00

*There is a good correlation when the correlation coefficient is greater than 0.7

Table 10 Rotation factor load matrix of chemical components in groundwater

	Factor 1	Factor 2
pH	−0.03	0.77*
EC (μs/cm)	0.83*	0.39
HCO_3^- (mg/L)	0.11	0.88*
Cl^- (mg/L)	0.88*	0.01
NO_3^- (mg/L)	0.87*	−0.32
SO_4^{2-} (mg/L)	0.83*	−0.22
Ca^{2+} (mg/L)	0.77*	0.47
Mg^{2+} (mg/L)	0.84*	0.22
$K^+ + Na^+$ (mg/L)	0.89*	0.21
Contribution rate (%)	57.338	20.444
Cumulative contribution rate (%)	57.338	77.782

*The ion with contribution rate greater than 0.75 is main ion

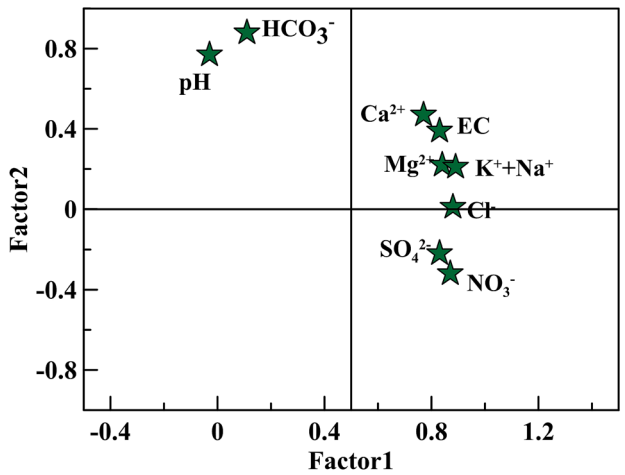

Fig. 9 Bivariate plots showing the relationships of the first two factor loadings (varimax rotated)

aquifer, calcite, and fluorite precipitate, which makes Ca^{2+} in groundwater of Qh^{al} aquifer decreased. Groundwater chemistry is largely dependent on the composition of water–rock interaction (Halim et al. 2010; Mukherjee et al. 2009; Verma et al. 2016).

Chloride is generally considered to be conservative in the most groundwater circumstances (Davis et al. 1998). The average concentration of Cl^- in Ey aquifer reaches 160.70 mg/L, and is 1.7 times higher than that in the other two aquifers, which may be caused by the dissolution of some chlorine bearing minerals (such as halite) in red sandstone (Fig. 6a) (Gan et al. 2014). Similar average values of Cl^- levels in Qh^{al} aquifer and Qp_3^{al} aquifer (i.e., 92.02 and 94.73 mg/L) indicates that the chlorine of the groundwater in the two aquifers may have the same source. The relationship between Cl^-/Br^- ratio and Cl^- concentration of groundwater in the three aquifers show that there is a positive correlation between the Cl^-/Br^- ratio and the Cl^- concentration. The near constant ratio between Cl^-/Br^- and Cl^- suggests a single dominant source of Cl^- (Davis et al. 1998). The Cl^-/Br^- increases with the increase of Cl^-, and, moreover, there are two different slopes obviously, which indicate that the chlorine of the groundwater in the study area may have two sources. The chlorine in Ey may originate from dissolution of saline minerals (such as halite) in red sandstone, and chlorine in Qp_3^{al} and Qh^{al} may come from atmospheric rainfall. Distinctive Cl/Br ratio helps to reconstruct the history of many groundwater systems (Davis et al. 1998; McArthur et al. 2012).

In addition, the Fitting-regression results of D-O isotopes show that the evaporation slopes (K) of the three aquifers are smaller than that of LMWL obviously, and most groundwater samples are distributed above the LMWL, which illustrate that the evaporation intensity of groundwater in the study area is lower than that of atmospheric precipitation. In addition, in the three aquifers, the evaporation intensity appears to be Qh^{al} aquifer > Qp_3^{al} aquifer > Ey aquifer, which decreases with the increase of burial depth, indicating that there is a certain degree of correlation between evaporation intensity and burial depth (Katz et al. 1997).

Results of principal component analysis for three aquifers showed that two factors were selected from Qp_3^{al} and Qh^{al} aquifers, but three factors were selected from Ey aquifer.

Table 11 Analysis of main ion and contribution rate in different aquifers

Aquifer	Factor 1		Factor 2		Factor 3	
	Main ion	Contribution rate (%)	Main ion	Contribution rate (%)	Main ion	Contribution rate (%)
Qh^{al}	EC, HCO_3^-, Cl^-, SO_4^{2-}, Ca^{2+}, Mg^{2+}, $K^+ + Na^+$	68.511	NO_3^-	19.453	–	–
Qp_3^{al}	EC, Cl^-, NO_3^-, SO_4^{2-}, Ca^{2+}, Mg^{2+}, $K^+ + Na^+$	58.172	HCO_3^-	17.253	–	–
Ey	EC, Cl^-, Ca^{2+}, Mg^{2+}	51.775	pH, SO_4^{2-}, $K^+ + Na^+$	20.506	NO_3^-	12.354

The components of the two factors in Qp_3^{al} and Qh^{al} aquifers are very similar, which indicates that the circumstances of groundwater in the two aquifers may be more similar (Mertler and Reinhart. 2016; Gan et al. 2018). Moreover, NO_3^- was sorted into factor 2 and factor 1 in Qh^{al} and Qp_3^{al} aquifers, respectively, while it was sorted into factor 3 in Ey aquifer, indicating a least affection of anthropogenic activities in Ey aquifer.

Conclusions

Using hydrochemistry, isotope, principal component analysis, and inverse geochemistry modeling, this study analyzes the hydro-geochemical evolution characteristics of shallow groundwater in the northeast of Jianghan Plain, which not only strengthens the understanding of groundwater evolution in this area, but also provides a reference for groundwater analysis in other similar areas.

The hydro-chemical type, composition, ion relationship, and evolution law of the three aquifers were analyzed detailedly. Hydro chemical types, anions and cations are more diversified in the Qh^{al} aquifer. When groundwater flows between Qp_3^{al} aquifer and Qh^{al} aquifer, calcite and fluorite precipitate, which makes Ca^{2+} in groundwater of Qh^{al} aquifer decreased. This indicates that water–rock interaction is one of the factors controlling the chemical evolution of groundwater. The relatively higher concentrations of Na^+ and Cl^- in Ey aquifer may be caused by the dissolution of saline minerals (such as halite) in red sandstone. The relationship of evaporation intensity in the three aquifers (i.e., Qh^{al} aquifer > Qp_3^{al} aquifer > Ey aquifer) studied by isotope analysis indicates that the evaporation intensity decreases with the increase of burial depth. The effecting factors and possible sources of groundwater chemical composition were explored by principal component analysis. The groundwater environment of Qp_3^{al} and Qh is very similar, and there is a close hydraulic connection between them. Anthropogenic activities may have a greater impact on the Qh^{al} aquifer, but a less impact on the Ey aquifer.

Supplementary Information The online version contains supplementary material available at https://doi.org/10.1007/s13146-021-00739-0.

Acknowledgements This research is supported by the National High Technology Research and Development Program of China (No. 2007AA06Z418), the National Natural Science Foundation of China (Nos. 20577036, 20777058, 20977070), the National Natural Science Foundation of Hubei province in China (No. 2015CFA137), China Geological Survey (DD20160290), and the Open Fund of Hubei Biomass-Resource Chemistry and Environmental Biotechnology Key Laboratory, and the Fund of Eco-environment Technology R&D and Service Center (Wuhan University).

Data availability statement All relevant data are included in the paper or Supplementary Information.

Declarations

Conflict of interest The authors declare no conflict of interest.

References

Adiya T, Johnson CL, Loewen MA, Ritterbush KA, Constenius KN, Dinter CM (2017) Microbial-caddisfly bioherm association from the lower cretaceous shinekhudag formation, Mongolia: earliest record of plant armoring in fossil caddisfly cases. PLoS ONE 12(11):e0188194. https://doi.org/10.1371/journal.pone.0188194

Al-Mashakbeh HM (2017) The influence of lithostratigraphy on the type and quality of stored water in Mujib Reservoir-Jordan. J Environ Prot 8(04):568–590. https://doi.org/10.4236/jep.2017.84038

Andersen MS, Nyvang V, Jakobsen R, Postma D (2005) Geochemical processes and solute transport at the seawater/freshwater interface of a sandy aquifer. Geochim Cosmochim Acta 69(16):3979–3994. https://doi.org/10.1016/j.gca.2005.03.017

Aravena R, Suzuki O (1990) Isotopic evolution of river water in the northern Chile region. Water Resour Res 26(12):2887–2895. https://doi.org/10.1029/WR026i012p02887

Ayadi Y, Mokadem N, Besser H, Khelifi F, Harabi S, Hamad A, Boyce A, Laouar R, Hamed Y (2018) Hydrochemistry and stable isotopes ($\delta^{18}O$ and $\delta^{2}H$) tools applied to the study of karst aquifers in southern mediterranean basin (Teboursouk area, NW Tunisia). J Afr Earth Sci 137:208–217. https://doi.org/10.1016/j.jafrearsci.2017.10.018

Barnes CJ, Allison GB (1988) Tracing of water movement in the unsaturated zone using stable isotopes of hydrogen and oxygen. J Hydrol 100(1–3):143–176. https://doi.org/10.1016/0022-1694(88)90184-9

Blasch KW, Bryson JR (2007) Distinguishing sources of ground water recharge by using $\delta^{2}H$ and $\delta^{18}O$. Ground Water 45(3):294–308. https://doi.org/10.1111/j.1745-6584.2006.00289.x

Bretzler A, Osenbruck K, Gloaguen R, Ruprecht JS, Kebede S, Stadler S (2011) Groundwater origin and flow dynamics in active rift systems—a multi-isotope approach in the Main Ethiopian Rift. J Hydrol 402(3–4):274–289. https://doi.org/10.1016/j.jhydrol.2011.03.022

Cates DA, Knox RC, Sabatini DA (1996) The impact of ion exchange processes on subsurface brine transport as observed on Piper diagrams. Ground Water 34(3):532–544. https://doi.org/10.1111/j.1745-6584.1996.tb02035.x

Chadha DK (1999) A proposed new diagram for geochemical classification of natural waters and interpretation of chemical data. Hydrogeol J 7(5):431–439. https://doi.org/10.1007/s100400050216

Christophersen N, Hooper RP (1992) Multivariate analysis of stream water chemical data: the use of principal components analysis for the end-member mixing problem. Water Resour Res 28(1):99–107. https://doi.org/10.1029/91WR02518

Clark I, Fritz P (1997) Environmental isotopes in hydrogeology. Lewis, New York

Davis SN, Whittemore DO, Fabrykamartin J (1998) Uses of chloride/bromide ratios in studies of potable water. Ground Water 36(2):338–350. https://doi.org/10.1111/j.1745-6584.1998.tb01099.x

Du Y, Ma T, Deng Y, Shen S, Lu Z (2017) Sources and fate of high levels of ammonium in surface water and shallow groundwater of the Jianghan Plain, Central China. Environ Sci-Process Impacts 19(2):161–172. https://doi.org/10.1039/c6em00531d

Du Y, Deng Y, Ma T, Lu Z, Shen S, Gan Y, Wang Y (2018a) Hydrogeochemical evidences for targeting sources of safe groundwater supply in arsenic-affected multi-level aquifer systems. Sci Total Environ 645:1159–1171. https://doi.org/10.1016/j.scitotenv.2018.07.173

Du Y, Ma T, Deng Y, Shen S, Lu Z (2018b) Characterizing groundwater/surface-water interactions in the interior of Jianghan Plain, central China. Hydrogeol J 26(4):1047–1059. https://doi.org/10.1007/s10040-017-1709-7

Gan Y, Wang Y, Duan Y, Deng Y, Guo X, Ding X (2014) Hydrogeochemistry and arsenic contamination of groundwater in the Jianghan Plain, central China. J Geochem Explor. https://doi.org/10.1016/j.gexplo.2013.12.013

Gan YQ, Zhao K, Deng YM, Liang X, Ma T, Wang YX (2018) Groundwater flow and hydro-geochemical evolution in the Jianghan Plain, central China. Hydrogeol J 26(5):1609–1623. https://doi.org/10.1007/s10040-018-1778-2

Gomaah M, Meixner T, Korany EA, Garamoon H, Gomaa MA (2016) Identifying the sources and geochemical evolution of groundwater using stable isotopes and hydrogeochemistry in the Quaternary aquifer in the area between Ismailia and El Kassara canals Northeastern Egypt. Arab J Geosci 9(6):437. https://doi.org/10.1007/s12517-016-2444-4

Halim MA, Majumder RK, Nessa SA, Hiroshiro Y, Sasaki K, Saha BB, Saepuloh A, Jinno K (2010) Evaluation of processes controlling the geochemical constituents in deep groundwater in Bangladesh: spatial variability on arsenic and boron enrichment. J Hazard Mater 180(1–3):50–62. https://doi.org/10.1016/j.jhazmat.2010.01.008

Harford CL, Sparks RSJ (2001) Recent remobilisation of shallow-level intrusions on Montserrat revealed by hydrogen isotope composition of amphiboles. Earth Planet Sci Lett 185(3–4):285–297. https://doi.org/10.1016/S0012-821X(00)00373-3

Huang P, Wang X (2018) Piper-PCA-fisher recognition model of water inrush source: a case study of the Jiaozuo Mining Area. Geofluids 2018:1–10. https://doi.org/10.1155/2018/9205025

Jiang X, Wan L, Wang X, Wang D, Wang H, Wang J, Zhang H, Zhang Z, Zhao K (2018) A multi-method study of regional groundwater circulation in the Ordos Plateau NW China. Hydrogeol J 26(5):1657–1668. https://doi.org/10.1007/s10040-018-1731-4

Katz BU, Coplen TB, Sullen TD (1997) Use of chemical and isotopic tracers to characterize the interactions between ground water and surface water in Mantled Karst. Ground Water 35:1014–1028. https://doi.org/10.1111/j.1745-6584.1997.tb00174.x

Kazakis N, Mattas C, Pavlou A, Patrikaki O, Voudouris K (2017) Multivariate statistical analysis for the assessment of groundwater quality under different hydrogeological regimes. Environ Earth Sci 76(9):349. https://doi.org/10.1007/s12665-017-6665-y

Khalil MM, Tokunaga T, Yousef AF (2015) Insights from stable isotopes and hydrochemistry to the Quaternary groundwater system, south of the Ismailia canal, Egypt. J Hydrol 527:555–564. https://doi.org/10.1016/j.jhydrol.2015.05.024

Lecomte KL, Pasquini AI, Depetris PJ (2005) Mineral weathering in a semiarid mountain river: its assessment through PHREEQC inverse modeling. Aquat Geochem 11(2):173–194. https://doi.org/10.1007/s10498-004-3523-9

Lihe Y, Guangcai H, Zhengping T, Ying L (2010) Origin and recharge estimates of groundwater in the ordos plateau, People's Republic of China. Environ Earth Sci 60(8):1731–1738. https://doi.org/10.1007/s12665-009-0310-3

McArthur JM, Sikdar PK, Hoque MA, Ghosal U (2012) Waste-water impacts on groundwater: Cl/Br ratios and implications for arsenic pollution of groundwater in the Bengal Basin and Red River Basin, Vietnam. Sci Total Environ 437:390–402. https://doi.org/10.1016/j.scitotenv.2012.07.068

McGuire KJ, DeWalle DR, Gburek WJ (2002) Evaluation of mean residence time in subsurface waters using oxygen-18 fluctuations during drought conditions in the mid-Appalachians. J Hydrol 261(1–4):132–149. https://doi.org/10.1016/S0022-1694(02)00006-9

Mertler CA, Reinhart RV (2016) Advanced and multivariate statistical methods: practical application and interpretation, 6th edn. Routledge, New York

Mokadem N, Demdoum A, Hamed Y, Bouri S, Hadji R, Boyce AJ, Laouar R, Sâad A (2016) Hydrogeochemical and stable isotope data of groundwater of a multi-aquifer system: Northern Gafsa basin–Central Tunisia. J Afr Earth Sci 114:174–191. https://doi.org/10.1016/j.jafrearsci.2015.11.010

Momen B, Eichler LW, Boylen CW, Zehr JP (1996) Application of multivariate statistics in detecting temporal and spatial patterns of water chemistry in Lake George, New York. Ecol Model 91(1–3):183–192. https://doi.org/10.1016/0304-3800(95)00189-1

Mountadar S, Younsi A, Hayani A, Siniti M, Tahiri S (2018) Groundwater salinization process in the coastal aquifer Sidi Abed-Ouled Ghanem (Province of El Jadida, Morocco). J Afr Earth Sci 147:169–177. https://doi.org/10.1016/j.jafrearsci.2018.06.025

Mukherjee A, Bhattacharya P, Shi F, Fryar AE, Mukherjee AB, Xie ZM, Jacks G, Bundschuh J (2009) Chemical evolution in the high arsenic groundwater of the Huhhot basin (Inner Mongolia, PR China) and its difference from the western Bengal basin (India). Appl Geochem 24(10):1835–1851. https://doi.org/10.1016/j.apgeochem.2009.06.005

Niu B, Wang H, Loáiciga HA, Hong S, Shao W (2017) Temporal variations of groundwater quality in the Western Jianghan Plain, China. Sci Total Environ 578:542–550. https://doi.org/10.1016/j.scitotenv.2016.10.225

Qin D, Turner JV, Pang Z (2005) Hydrogeochemistry and groundwater circulation in the Xi'an geothermal field. China Geotherm 34(4):471–494. https://doi.org/10.1016/j.geothermics.2005.06.004

Rodriguez M, Sfer A, Sales A (2016) Application of chemometrics to hydrochemical parameters and hydrogeochemical modeling of Calera River basin in the Northwest of Argentina. Environ Earth Sci 75(6):500. https://doi.org/10.1007/s12665-016-5328-8

Sharif MU, Davis RK, Steele KF, Kim B, Kresse TM, Fazio JA (2008) Inverse geochemical modeling of groundwater evolution with emphasis on arsenic in the Mississippi River Valley alluvial aquifer, Arkansas (USA). J Hydrol 350(1–2):41–55. https://doi.org/10.1016/j.jhydrol.2007.11.027

Shi D, Yin X, Sun J, Yin Z (1998) A simulation study on the evolution of groundwater circulation systems in Cenozoic basins of Northern China. Acta Geol Sin 72(1):100–107. https://doi.org/10.1111/j.1755-6724.1998.tb00737.x

Slimani R, Guendouz A, Trolard F, Moulla AS, Hamdi-Aïssa B, Bourrié G (2017) Identification of dominant hydrogeochemical processes for groundwaters in the Algerian Sahara supported by inverse modeling of chemical and isotopic data. Hydrol Earth Syst Sci 21(3):1669–1691. https://doi.org/10.5194/hess-21-1669-2017

Van Geldern R, Baier A, Subert HL, Kowol S, Balk L, Barth JA (2014) Pleistocene paleo-groundwater as a pristine fresh water resource in southern Germany–evidence from stable and radiogenic isotopes. Sci Total Environ 496:107–115. https://doi.org/10.1016/j.scitotenv.2014.07.011

Verma S, Mukherjee A, Mahanta C, Choudhury R, Mitra K (2016) Influence of geology on groundwater–sediment interactions in arsenic enriched tectono-morphic aquifers of the Himalayan Brahmaputra River basin. J Hydrol 540:176–195. https://doi.org/10.1016/j.jhydrol.2016.05.041

Weyhenmeyer CE, Burns SJ, Waber HN, Macumber PG, Matter A (2002) Isotope study of moisture sources, recharge areas, and groundwater flow paths within the eastern Batinah coastal plain Sultanate of Oman. Water Resour Res 38(10):21–222. https://doi.org/10.1029/2000WR000149

Williams AE, Rodoni DP (1997) Regional isotope effects and application to hydrologic investigations in southwestern California. Water Resour Res 33(7):1721–1729. https://doi.org/10.1029/97WR01035

Yang N, Wang G, Shi Z, Zhao D, Jiang W, Guo L, Liao F, Zhou P (2018) Application of multiple approaches to investigate the hydrochemistry evolution of groundwater in an Arid Region: Nomhon Northwestern China. Water 10(11):1667. https://doi.org/10.3390/w10111667

Yang J, Ye M, Tang Z, Jiao T, Song X, Pei Y, Liu H (2020) Using cluster analysis for understanding spatial and temporal patterns and controlling factors of groundwater geochemistry in a regional aquifer. J Hydrol 583:124594. https://doi.org/10.1016/j.jhydrol.2020.124594

Yangui H, Zouari K, Trabelsi R, Rozanski K (2011) Recharge mode and mineralization of groundwater in a semi-arid region: Sidi Bouzid plain (central Tunisia). Environ Earth Sci 63(5):969–979. https://doi.org/10.1007/s12665-010-0771-4

Ye C, Zheng M, Wang Z, Hao W, Wang J, Lin X, Han J (2015) Hydrochemical characteristics and sources of brines in the Gasikule salt lake, Northwest Qaidam Basin China. Geochem J 49(5):481–494. https://doi.org/10.2343/geochemj.2.0372

Yidana SM, Ophori D, Banoeng-Yakubo B (2008) A multivariate statistical analysis of surface water chemistry data—the Ankobra Basin Ghana. J Environ Manage 86(1):80–87. https://doi.org/10.1016/j.jenvman.2006.11.023

Zeng Z (1997) The background features and formation of chemical elements of groundwater in the region of the middle and lower reaches of the Yangtze River. Acta Geol Sin 71(1):80–89. https://doi.org/10.1111/j.1755-6724.1997.tb00348.x

Zhang Y, Tian Y, Shen M, Zeng G (2018) Heavy metals in soils and sediments from Dongting Lake in China: occurrence, sources, and spatial distribution by multivariate statistical analysis. Environ Sci Pollut Res 25(14):13687–13696. https://doi.org/10.1007/s11356-018-1590-5

Zhou Y, Wang Y, Li Y, Zwahlen F, Boillat J (2013) Hydrogeochemical characteristics of central Jianghan Plain China. Environ Earth Sci 68(3):765–778. https://doi.org/10.1007/s12665-012-1778-9

Publisher's Note Springer Nature remains neutral with regard to jurisdictional claims in published maps and institutional affiliations.